Inorganic Chemistry

Article

pubs.acs.org/IC

Structure and Magnetism of the Topotactically Reduced Oxychloride $Sr_4Mn_3O_{6.5}Cl_2$

Fabio Denis Romero and Michael A. Hayward*

Inorganic Chemistry Laboratory, Department of Chemistry, University of Oxford, South Parks Road, Oxford, OX1 3QR, United Kingdom

ABSTRACT: Reaction of the n = 3 Ruddlesden–Popper oxychloride $Sr_4Mn_3O_{7.5}Cl_2$ with calcium hydride yields the topotactically reduced phase $Sr_4Mn_3O_{6.5}Cl_2$. The deintercalation of oxide ions from the central $MnO_{1.5}$ layer of the starting phase is accompanied by a rearrangement of the anion lattice, resulting in a layer of composition $MnO_{0.5}$ in the reduced material, consisting of chains of MnO_4 tetrahedra connected by edge and corner sharing. Magnetization and low-temperature neutron diffraction data are consistent with antiferromagnetic coupling of manganese spins, but no long-range magnetic order is observed down to 5 K, presumably due to the large interlayer separation in the reduced phase. The influence of anion substitution on the structural selectivity of low-temperature reduction reactions is discussed.

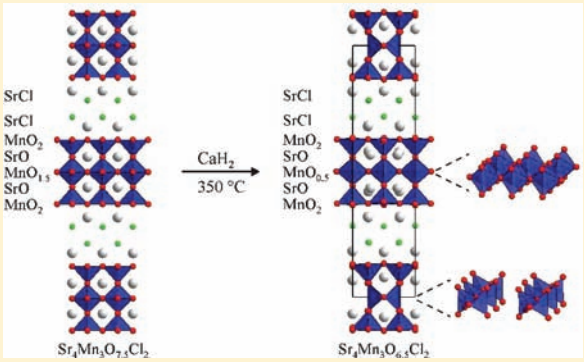

INTRODUCTION

The low-temperature topotactic reduction of complex transition-metal oxides offers an efficient synthetic route for the preparation of highly metastable phases inaccessible by high-temperature methods. As these low-temperature reactions are performed under kinetic rather than thermodynamic control, phases containing transition-metal cations in highly unusual oxidation states and/or coordination geometries can be readily prepared,[1−4] offering chemists the opportunity to study the electronic and magnetic behavior of these species in extended oxide lattices.

In order to maximize the potential of this low-temperature synthetic approach, a degree of structural and compositional control is required to direct reactions toward the preparation of target phases and thus move from synthesis by discovery, typical of solid-state chemistry, to synthesis by rational design, more typical of the preparation of molecules. We have previously demonstrated that the non-transition-metal "A-cations" present in complex transition-metal oxide phases can exert considerable influence over the product phases prepared by low-temperature reduction reactions. For example, the reduction of the isostructural and isoelectronic A-cation ordered phases $YBaCo_2O_5$ and $LaBaCo_2O_5$ with NaH yields $YBaCo_2O_{4.5}$ and $LaBaCo_2O_{4.25}$, respectively.[5] These two reduced phases have different compositions and anion-vacancy ordering schemes, despite starting from isoelectronic and isostructural substrate phases, demonstrating the influence of the Ln^{3+} "A-cations" on the outcome of low-temperature reduction reactions.

Building on these cation-directed syntheses, we have recently extended our investigations to study the influence of anion substitutions on the selectivity of reduction reactions. The structures of $A_{n+1}B_nO_{3n+1}$ Ruddlesden–Popper oxide phases can be described as the stacking of AO and BO_2 layers in a $-AO-[AO-BO_2]_n-$ stacking sequence. The resulting structures consist of BO_6 octahedra arranged in perovskite blocks n octahedra thick separated by AO rocksalt layers, as shown in Figure 1.[6] The oxide ions within the rocksalt layers of Ruddlesden–Popper phases can be readily replaced by halogens, most commonly chlorine, to form layered oxyhalide phases as shown in Figure 1.[7−9] Previous work has shown that this partial replacement of oxide ions with halide ions can change the anion vacancy order present in reduced product phases, in comparison to all-oxide analogues. For example, reduction of the n = 2 Ruddlesden–Popper phases $Sr_3Fe_2O_7$ and $Sr_3Fe_2O_5Cl_2$ with hydride reducing agents yields the respective Fe^{2+} phases $Sr_3Fe_2O_5$ and $Sr_3Fe_2O_4Cl_2$ (Figure 1).[10,11] Both of these phases contain arrays of apex-linked square-planar $Fe^{II}O_4$ units; however, in the all-oxide phase $Sr_3Fe_2O_5$ these FeO_4 polyhedra from one-dimensional chains, while in the oxychloride phase $Sr_3Fe_2O_4Cl_2$ the FeO_4 units form two-dimensional sheets, demonstrating the structure-directing influence of the substituted anions.

In this current report we have extended our study to investigate the reduction chemistry of the n = 3 Ruddlesden–Popper oxychloride $Sr_4Mn_3O_{7.5}Cl_2$.[7,8] This phase can be related to the hypothetical n = 3 Ruddlesden–Popper oxide $Sr_4Mn_3O_{10}$ as shown in Figure 2; however, the presence of chloride ions appears to limit the manganese oxidation state to a value of Mn^{3+}, resulting in oxide ion vacancies within the central perovskite layer. As a result the structure of $Sr_4Mn_3O_{7.5}Cl_2$ can be described as the stacking of AX (X = O, Cl) and $MnO_{1.5}$ layers as shown in Figure 2.

Received: February 3, 2012
Published: April 23, 2012

   dx.doi.org/10.1021/ic300258f | *Inorg. Chem.* 2012, 51, 5325−5331

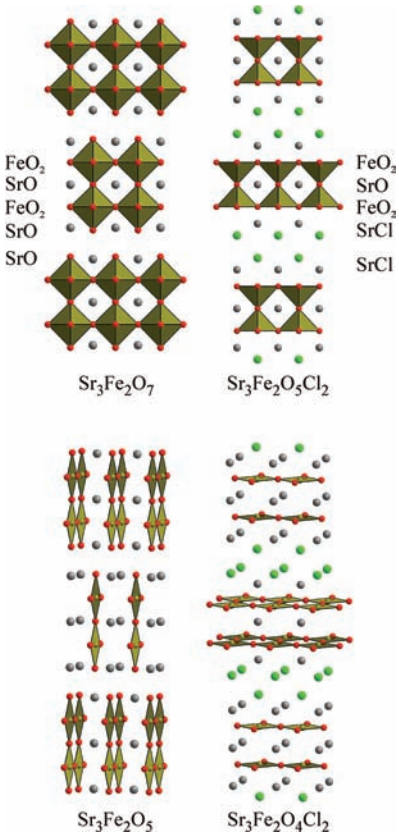

Figure 1. Crystal structures of $Sr_3Fe_2O_7$, $Sr_3Fe_2O_5Cl_2$, $Sr_3Fe_2O_5$, and $Sr_3Fe_2O_4Cl_2$.

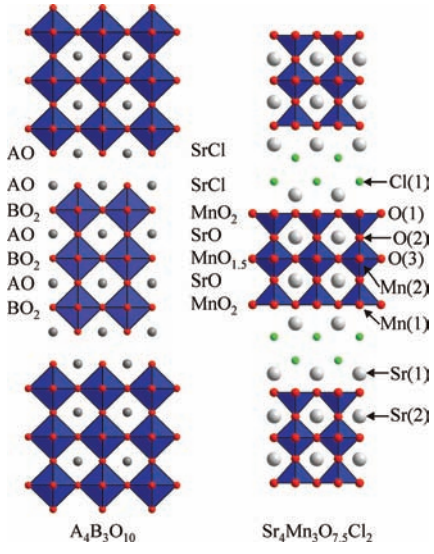

Figure 2. Structures of the $n = 3$ Ruddlesden–Popper phases $A_4B_3O_{10}$ and $Sr_4Mn_3O_{7.5}Cl_2$.

EXPERIMENTAL SECTION

Synthesis of $Sr_4Mn_3O_{7.5}Cl_2$. Samples of $Sr_4Mn_3O_{7.5}Cl_2$ were prepared by the method described previously by Knee et al.[7,8] Suitable stoichiometric ratios of SrO (prepared from the decomposition of $SrCO_3$ at 975 °C under vacuum), Mn_2O_3 (prepared by heating MnO_2 at 650 °C under flowing argon) and a 10% excess of $SrCl_2$ (dried at 160 °C under vacuum) were ground together in an argon-filled glovebox (O_2 and H_2O <1 ppm) and sealed under vacuum in a silica tube. The reagents were then heated at 850 °C for two periods of 2 days with an intermediate regrinding. Once the reaction was observed to be complete, excess $SrCl_2$ was removed by washing the sample with a 1:1 water:methanol mixture and then filtering. X-ray powder diffraction data collected from the washed sample (Figure 3)

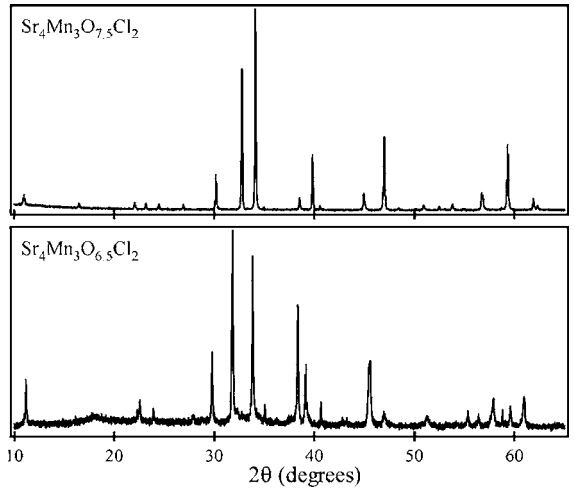

Figure 3. X-ray powder diffraction data collected from (top) $Sr_4Mn_3O_{7.5}Cl_2$ and (bottom) $Sr_4Mn_3O_{6.5}Cl_2$.

could be readily indexed using a tetragonal unit cell with lattice parameters ($a = 3.864(7)$ Å, $c = 32.244(1)$ Å), in good agreement with published values.[7,8]

Reduction of $Sr_4Mn_3O_{7.5}Cl_2$. The reduction of $Sr_4Mn_3O_{7.5}Cl_2$ was performed using CaH_2 as a solid-state reducing agent. In order to investigate the reactivity of $Sr_4Mn_3O_{7.5}Cl_2$ and CaH_2 as a function of temperature, small-scale (~300 mg) reactions were performed. Samples were prepared as 4:1 stoichiometric ratios of CaH_2:$Sr_4Mn_3O_{7.5}Cl_2$, thoroughly mixed in an argon-filled glovebox and then sealed in evacuated Pyrex ampoules. Samples were then heated at a series of different temperatures for two periods of 2 days, with intermediate regrinding.

Due to the hazards associated with the production of hydrogen gas when using CaH_2 as a reducing agent,[12] large samples suitable for characterization by neutron powder diffraction were synthesized in a sealed Parr Series 4740 pressure vessel, which is capable of withstanding the hydrogen gas pressures generated by these reactions. Approximately 4 g of $Sr_4Mn_3O_{7.5}Cl_2$ was mixed in an argon-filled glovebox with 4 mol equiv of CaH_2 and loaded into a silica finger, which was then sealed inside the pressure vessel. The pressure vessel was then evacuated and heated so that the sample was held at a temperature of 350 °C for 4 periods of 2 days with intermediate grinding. After the reaction, samples were washed under nitrogen with 4 × 100 mL aliquots of 0.1 M NH_4Cl in methanol to remove any calcium-containing phases (CaH_2 and CaO) and then washed with a further 4 × 100 mL aliquots of clean methanol before being dried under vacuum.

Characterization. X-ray powder diffraction data were collected from samples contained within homemade gas-tight sample holders using a PANalytical X'Pert diffractometer incorporating an X'celerator position sensitive detector (monochromatic Cu $K\alpha_1$ radiation). Neutron powder diffraction data were collected from samples contained within vanadium cans, which had been sealed under argon with indium washers, using the D2B diffractometer ($\lambda = 1.59$ Å) at the ILL neutron source, Grenoble, France. Rietveld profile refinement was performed using the GSAS suite of programs.[13] Electron diffraction data were collected from finely ground samples supported on lacy carbon grids (deposited from suspension in methanol) using a JEOL 2000FX microscope operating at 200 kV. Magnetization measurements were collected using a Quantum Design MPMS SQUID magnetometer. Iodometric titrations were performed to determine the exact oxygen stoichiometry of reduced phases by dissolving samples in HCl containing an excess of KI and titrating the liberated I_2 with $Na_2S_2O_3$.

dx.doi.org/10.1021/ic300258f | Inorg. Chem. 2012, 51, 5325–5331

RESULTS

Small-scale tests of the reactivity of $Sr_4Mn_3O_{7.5}Cl_2$ with CaH_2 revealed that at temperatures below 300 °C there is no reaction. However, at 350 °C, the reaction between $Sr_4Mn_3O_{7.5}Cl_2$ and CaH_2 yielded a new tetragonal phase with lattice parameters a = 3.987(2) Å and c = 32.047(2) Å (according to X-ray powder diffraction data, Figure 3), suggesting a topotactic reduction reaction had occurred. Iodometric titrations indicate this new phase has a composition of $Sr_4Mn_3O_{6.5}Cl_2$. Reactions at temperatures above 400 °C led to sample decomposition.

Structural Characterization. Given the apparent similarity between the structures of $Sr_4Mn_3O_{7.5}Cl_2$ and $Sr_4Mn_3O_{6.5}Cl_2$ from comparison of the X-ray powder diffraction data shown in Figure 3, a model based on the reported structure of $Sr_4Mn_3O_{7.5}Cl_2$[8] was refined against neutron powder diffraction data collected from $Sr_4Mn_3O_{6.5}Cl_2$ at room temperature. In this preliminary structural refinement all atomic positional parameters, thermal displacement parameters, and fractional occupancies were allowed to vary. This initial refinement converged to yield a model which, with the exception of the central MnO_x layer in each perovskite block (see Figure 2), retained the structure of the $Sr_4Mn_3O_{7.5}Cl_2$ phase with all atomic sites fully occupied within error. Close inspection of the central MnO_x layer of this initial refined model revealed that the displacement parameters of the manganese cations within this layer were extremely large and that the fractional occupancies of anion sites within this layer had refined to unphysical negative values, indicating oxide ions had been removed from the central layer of this material during the reduction reaction. Furthermore, Fourier difference plots calculated from this initial refinement revealed an excess of scattering at ($^1/_2$, $^1/_2$, 0) within the disrupted central layer, indicating that a significant rearrangement of the anion lattice had occurred within this layer on reduction.

Close inspection of the fit to the diffraction data of the initial refinement revealed a number of diffraction peaks which could not be accounted for using the preliminary model. These additional peaks could be split into two groups: those which were attributable to the presence of impurity phases (MnO and CaH_2) and those which were not. This latter group of additional diffraction peaks indicates that the product phase has a larger/lower symmetry unit cell than $Sr_4Mn_3O_{7.5}Cl_2$.

In order to unambiguously determine the unit cell dimensions and space group symmetry of $Sr_4Mn_3O_{6.5}Cl_2$, electron diffraction data were collected. As shown in Figure 4, these data exhibit a series of diffraction spots consistent with a 2 × 2 × 1 unit cell expansion relative to the unit cell of $Sr_4Mn_3O_{7.5}Cl_2$. Analysis of the systematic absences of the electron diffraction data sets revealed extinction conditions consistent with space group $P4_2/mmc$.

Using the information above, a model based on the three-layer structure of $Sr_4Mn_3O_{7.5}Cl_2$ was constructed within an expanded 2 × 2 × 1 unit cell in space group $P4_2/mmc$. Guided by the Fourier difference plots, the anion sites present in the central layer of the $Sr_4Mn_3O_{7.5}Cl_2$ structure were replaced by sites at 4*l* (0, 0.25, 0) and 4*k* ($^1/_2$, 0.25, 0) within this new expanded model. These new anion sites were set to 50% occupancy to form a model with a composition of $Sr_4Mn_3O_{6.5}Cl_2$ in line with the titration data. Secondary phases corresponding to the structures of MnO and CaH_2 were also added to the model.

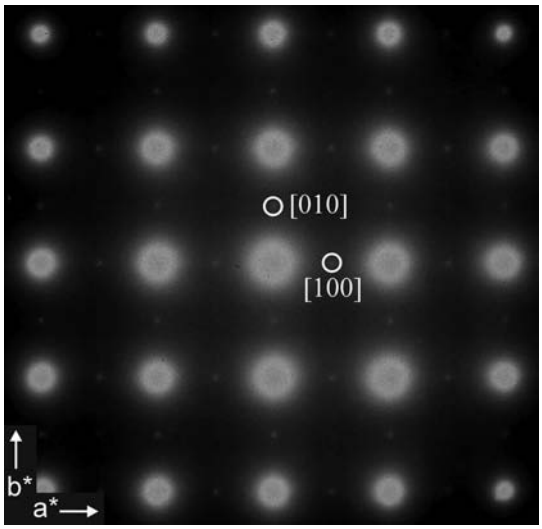

Figure 4. Electron diffraction data collected from the [001] zone of $Sr_4Mn_3O_{6.5}Cl_2$. Weak spots (circled) indicate that the unit cell has a 2 × 2 × 1 relationship to the unit cell of $Sr_4Mn_3O_{7.5}Cl_2$.

Refinement of this model was performed in two stages. Initially the positional and displacement parameters of all the atoms outside the central MnO_x layer were refined to relax the bulk structure. Subsequently the positional parameters, displacement parameters, and fractional occupancies of the atoms in the central layer were refined freely. This led to the anion site at 4*k* ($^1/_2$, ~0.25, 0) refining to full occupancy and the site at 4*l* (0, ~0.25, 0) refining to zero occupancy. The change in oxide occupancy was accompanied by a shift in the position of the manganese cations such that the central MnO_x layer has a stoichiometry of $MnO_{0.5}$ and consists of MnO_4 tetrahedra linked into chains by corner and edge sharing, with the chain propagation direction changing by 90° between adjacent three-layer blocks to maintain the overall tetragonal symmetry of the phase, as shown in Figure 5.

The refinement converged to give a good statistical fit (χ^2 = 1.49). Full details of the refined structure are detailed in Table 1, with selected bond lengths in Table 2. A plot of observed against calculated diffraction data is shown in Figure 6.

Magnetic Characterization. Magnetization data collected from $Sr_4Mn_3O_{6.5}Cl_2$ as a function of temperature over the range $5 \leq T/K \leq 300$ are shown in Figure 7. They reveal a small divergence between zero-field-cooled and field-cooled data over the whole measured temperature range. In spite of this divergence the zero-field-cooled data can be fitted by the Curie–Weiss law ($\chi = C/(T - \theta) + K$) in the temperature range $30 \leq T/K \leq 300$ to yield values of C = 2.63(4) cm^3 K mol^{-1}, θ = −18.7(5) K, and K = 0.0118(1) cm^3 mol^{-1}. Magnetization-field data collected at 300 K are linear and pass through the origin. In contrast, analogous data collected at 5 K (Figure 7) exhibit hysteresis and are displaced from the origin. Neutron diffraction data collected from $Sr_4Mn_3O_{6.5}Cl_2$ at 5 K show no evidence for long-range magnetic order.

DISCUSSION

The reaction of $Sr_4Mn_3O_{7.5}Cl_2$ with CaH_2 leads to the reduction of the oxychloride phase, resulting in a new material of composition $Sr_4Mn_3O_{6.5}Cl_2$. In the reduction process, oxide ions are reductively deintercalated from the central $MnO_{1.5}$ layer of the substrate phase (Figure 2), forming a new layer of

dx.doi.org/10.1021/ic300258f | Inorg. Chem. 2012, 51, 5325–5331

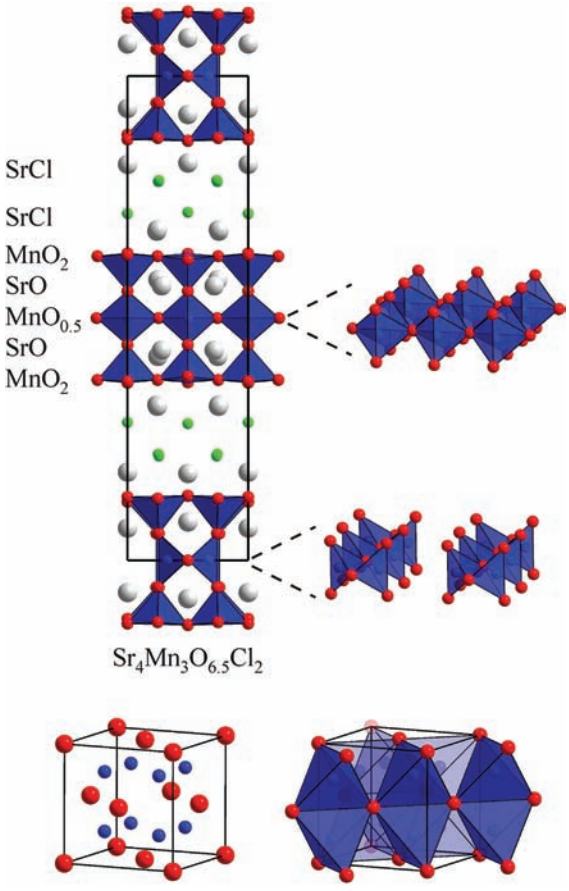

Figure 5. Structure of $Sr_4Mn_3O_{6.5}Cl_2$, highlighting the edge- and corner-linked MnO_4 tetrahedra (top) and a comparison to the polyhedral connectivity in the antifluorite structure (bottom).

Table 1. Structural Parameters from the Refinement of $Sr_4Mn_3O_{6.5}Cl_2$ against Neutron Powder Diffraction Data

atom	*x*	*y*	*z*	U_{iso} (Å^2)
Sr(1)	0	0.282(2)	0.0667(5)	0.0024(1)
Sr(2)	$^1/_2$	0.252(2)	0.794(6)	0.0024(1)
Sr(3)	0	0.247(5)	0.1825(9)	0.0024(1)
Sr(4)	$^1/_2$	0.243(5)	0.1797(8)	0.0024(1)
Mn(1)	0.263(1)	0	0.1250(4)	0.0010(2)
Mn(2)	0.249(1)	$^1/_2$	0.1253(4)	0.0010(2)
Mn(3)	0.328(1)	0	0	0.0054(3)
Mn(4)	0.327(1)	$^1/_2$	0	0.0054(3)
O(1)	0.259(1)	0	0.0557(4)	0.0031(3)
O(2)	0.239(1)	0	0.0556(4)	0.0031(3)
O(3)	0	0	0.131(2)	0.0010(1)
O(4)	$^1/_2$	0	0.134(2)	0.0010(1)
O(5)	0	$^1/_2$	0.121(1)	0.0010(1)
O(6)	$^1/_2$	$^1/_2$	0.133(2)	0.0010(1)
O(7)	0.250(5)	0.751(4)	0.128(1)	0.0010(1)
O(8)	$^1/_2$	0.256(3)	0	0.0045(3)
Cl(1)	0.261(5)	0	0.2158(6)	0.0008(1)
Cl(2)	0.255(4)	$^1/_2$	0.2184(7)	0.0008(1)

$Sr_4Mn_3O_{6.5}Cl_2$: space group $P4_2/mmc$, a = 7.9744(4) Å, c = 32.047(2) Å, weight fraction 87(1)%

MnO: space group $Fm\bar{3}m$, a = 4.446(1) Å, weight fraction 6(1)%

CaH_2: space group *Pnma*, a = 5.961(1) Å, b = 3.600(1) Å, c = 6.819(1) Å, weight fraction 7%

χ^2 = 1.493, wRp = 2.98%, Rp = 2.36%

Table 2. Selected Bond Lengths Extracted from the Refined Structure of $Sr_4Mn_3O_{6.5}Cl_2$

cation	anion	bond length (Å)
Mn(1)	O(1)	2.22(1)
	O(3)	2.10(1)
	O(4)	1.91(1)
	O(7)	2 × 1.99(3)
	Cl(1)	2.91(2)
Mn(2)	O(2)	2.23(1)
	O(5)	1.99(1)
	O(6)	2.01(1)
	O(7)	2 × 2.00(3)
	Cl(2)	2.98(2)
Mn(3)	O(1)	1.86(1)
	O(8)	2.45(2)
Mn(4)	O(2)	1.91(1)
	O(8)	2.38(2)
Sr(1)	O(1)	3.07(1)
	O(2)	2.60(1)
	O(3)	3.05(4)
	O(5)	2.46(2)
	O(7)	2 × 2.81(2)
Sr(2)	O(1)	2.88(1)
	O(2)	2.97(1)
	O(4)	2.66(4)
	O(6)	2.61(4)
	O(7)	2 × 2.53(3)
	O(8)	2.54(1)
Sr(3)	O(3)	2.57(5)
	O(5)	2.82(4)
	O(7)	2 × 2.65(4)
	Cl(1)	2 × 3.05(3)
	Cl(2)	2 × 3.08(3)
Sr(4)	O(4)	2.42(5)
	O(6)	2.53(5)
	O(7)	2 × 2.59(4)
	Cl(1)	2 × 2.95(3)
	Cl(2)	2 × 3.09(3)
Mn(3)–Mn(3)		2.74(1)
Mn(4)–Mn(4)		2.75(1)

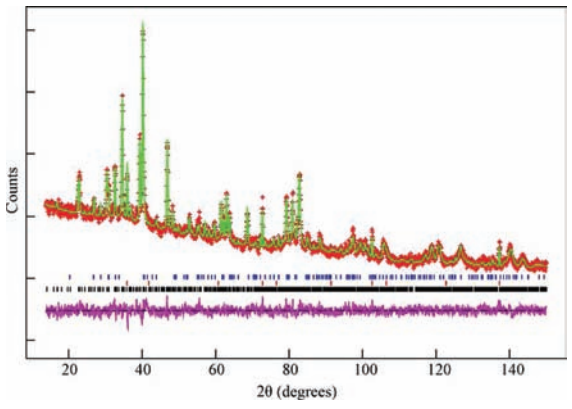

Figure 6. Observed, calculated, and difference plots from the structural refinement of $Sr_4Mn_3O_{6.5}Cl_2$ against neutron powder diffraction data. Tick marks correspond to the allowed peak positions of (top) CaH_2, (middle) MnO, and (bottom) $Sr_4Mn_3O_{6.5}Cl_2$.

composition $MnO_{0.5}$. The deintercalation is associated with a rearrangement of the anion lattice, such that the manganese

dx.doi.org/10.1021/ic300258f | *Inorg. Chem.* 2012, 51, 5325–5331

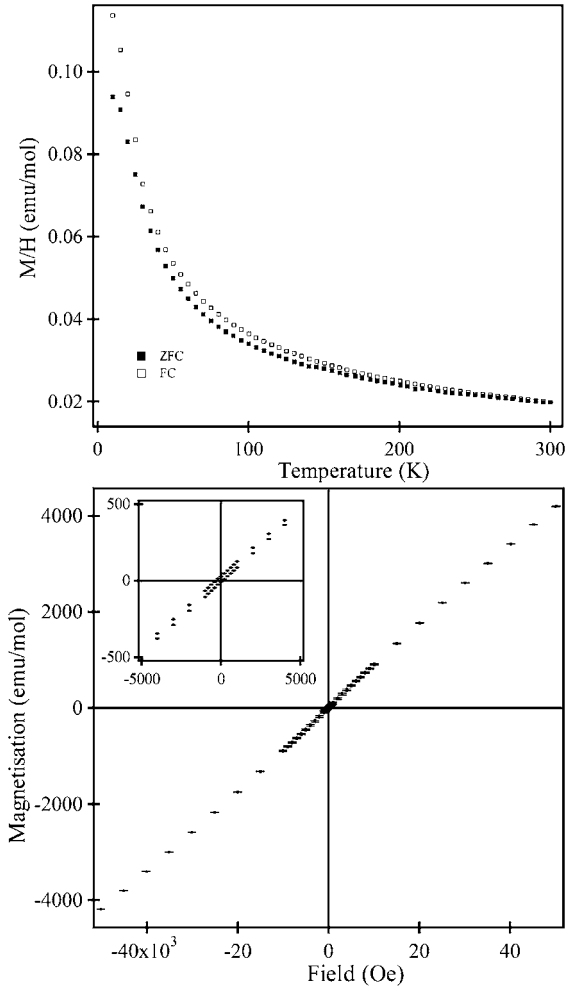

Figure 7. (top) Zero-field-cooled and field-cooled magnetization data collected from $Sr_4Mn_3O_{6.5}Cl_2$ as a function of temperature. (bottom) Magnetization-field data collected at 5 K. The inset shows that data are asymmetric about the origin.

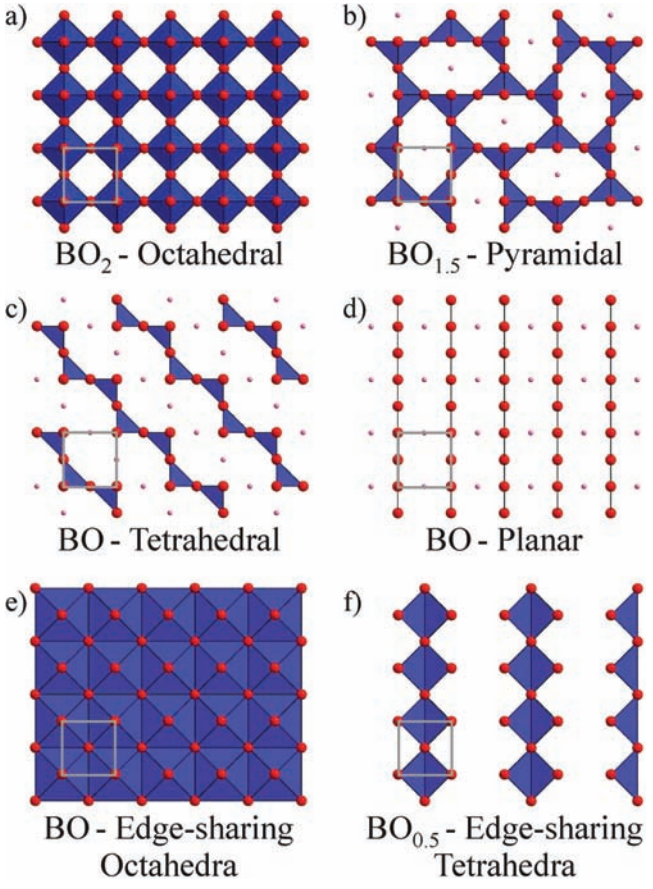

Figure 8. Common anion-vacancy ordering arrangements of BO_{2-x} layers in anion-deficient Ruddlesden–Popper and perovskite phases.

cations within the new $MnO_{0.5}$ layers are located in MnO_4 tetrahedra, which share corners and edges to form chains which run through the structure, as shown in Figure 5.

The anion-deficient $MnO_{0.5}$ sheets present in the structure of $Sr_4Mn_3O_{6.5}Cl_2$ are, to the best of our knowledge, unique among anion-deficient Ruddlesden–Popper phases. While there are a considerable number of anion-deficient Ruddlesden–Popper phases reported which, like $Sr_4Mn_3O_{6.5}Cl_2$, accommodate their anion deficiency as anion vacancies within BO_{2-x} layers, the BO_{2-x} layers in these other phases tend to have much lower anion-vacancy concentrations than the $MnO_{0.5}$ layer present in $Sr_4Mn_3O_{6.5}Cl_2$. Taking the three anion-deficient Ruddlesden–Popper phases $Ca_2MnO_{3.5}$,[14] $La_4Co_3O_9$,[15] and $Sr_3Fe_2O_5$[10] as examples of this point, we observe that the anion-deficient $n = 1$ Ruddlesden–Popper phase $Ca_2MnO_{3.5}$ accommodates anion vacancies within $MnO_{1.5}$ layers (Figure 8b), which are stacked with CaO rocksalt layers in a $-CaO-CaO-MnO_{1.5}-$ sequence. In contrast, the structures of both $La_4Co_3O_9$ and $Sr_3Fe_2O_5$ contain anion-deficient BO layers. The $n = 3$ Ruddlesden–Popper phase $La_4Co_3O_9$ has a $-LaO-LaO-CoO_2-LaO-CoO-LaO-CoO_2-$ stacking sequence in which the anion vacancies are ordered within CoO layers (Figure 8c) to form chains of corner-sharing CoO_4 tetrahedra akin to those present in $A_2B_2O_5$ brownmillerite phases.[16] The anion-deficient structure of $Sr_3Fe_2O_5$ has an $-SrO-SrO-FeO-SrO-FeO-$ stacking sequence, but in this case the anion vacancies are arranged to form corner-sharing FeO_4 square planes within the FeO layers (Figure 8d).

The anion-deficient BO_{2-x} layers in the three example phases shown can all be readily formed by the simple removal of oxide ions from stoichiometric BO_2 layers, as shown in Figure 8. This is not true of the $MnO_{0.5}$ layers in the structure of $Sr_3Mn_4O_{6.5}Cl_2$. These layers are instead derived from a layer of composition MnO, which has the same manganese lattice as the BO_{2-x} sheets in the Ruddlesden–Popper lattice, but in which the oxide ions are positioned in the middle of a square of manganese centers, such that the manganese cations reside in edge-sharing MnO_6 octahedra, as shown in Figure 8e. A layer of this type has been observed recently in $La_{1-x}Ca_xMnO_2$ phases prepared by the reduction of $La_{1-x}Ca_xMnO_3$ perovskites.[3] Removal of half the oxide ions from this MnO layer converts the sheet of edge-sharing octahedra into the chains of MnO_4 tetrahedra observed in the structure of $Sr_4Mn_3O_{6.5}Cl_2$ (Figure 8f).

It has been observed previously that the location of anion vacancies within topotactically reduced phases can be rationalized by considering the coordination preferences of all the metal cations within the host phase.[11,17] Following the logic described previously,[12] it can be seen that in order to best satisfy the competing coordination preferences of the strontium and manganese centers on the reduction of $Sr_4Mn_3O_{7.5}Cl_2$, oxide ions will be removed from anion sites with weak bonds to strontium and strong bonds to manganese. We can evaluate this

dx.doi.org/10.1021/ic300258f | Inorg. Chem. 2012, 51, 5325–5331

using bond valence sums (BVS),[18] which can provide us with crude, computationally cheap estimates of metal−anion bond strength. As shown in Table 3, the O(1) anion site of

Table 3. Bond Valence Sums Calculated for the Anion Sites of $Sr_4Mn_3O_{7.5}Cl_2$

	O(1)	O(2)	O(3)	Cl(1)
BVS(Mn)	1.202	1.21	1.216	0.083
BVS(Sr)	0.886	0.756	0.752	1.128
BVS(Mn) − BVS(Sr)	+0.316	+0.454	+0.464	−1.045

$Sr_4Mn_3O_{7.5}Cl_2$ has the smallest value of BVS(Mn) − BVS(Sr) of the three oxide ion sites, indicating that it is highly unfavorable to remove anions from this site on lattice energy grounds. This low value can be attributed to the presence of chloride ions in the rocksalt layers of $Sr_4Mn_3O_{7.5}Cl_2$ which move the Sr(1) cations toward the $Mn(1)(O(1))_2$ plane in order to maximize the Sr(1) bond valence sum (Sr(1)−O(1) = 2.56 Å,[8] equivalent bond length in $Sr_3Mn_2O_7$ 2.62 Å[19]). This acts to strengthen the Sr(1)−O(1) bonding "pinning" the oxide ions within the $Mn(1)(O(1))_2$ layer of $Sr_4Mn_3O_{7.5}Cl_2$ in place.

The BVS(Mn) − BVS(Sr) values for the two remaining anion sites, O(2) and O(3), are very similar, as shown in Table 3. However it should be noted that removal of oxide ions from the O(2) anion site would result in the formation of square-planar $Mn(1)(O(1))_4$ centers. While square-planar manganese centers are not completely unknown, they generally only occur when stabilized in some way — for example, when manganese cations are present as low-level dopants in the infinite layer phase $SrFeO_2$.[20,21] In the absence of external stabilization square-planar manganese centers can be considered disfavored. Thus, it can be seen that removal of oxide ions from the O(2) anion site is also disfavored. Therefore, by a process of elimination we can see that the only site from which anions can be removed, to yield a low-energy structure, is O(3), explaining the selective removal of oxide from the central MnO_x layers of $Sr_4Mn_3O_{7.5}Cl_2$ on reduction.

The extreme anion deficiency of the $MnO_{0.5}$ layer formed on reduction can be attributed to the large electrochemical reducing power of CaH_2. Previous studies have shown that CaH_2 has sufficient reducing power to topotactically reduce Ruddlesden−Popper manganates to Mn^{2+} phases (e.g., $LaSrMnO_{3.5}$[17]). If anions can only be removed from the O(3) anion site of $Sr_4Mn_3O_{7.5}Cl_2$, reduction of this phase to the theoretical Mn^{2+} phase $Sr_4Mn_3O_6Cl_2$ would require the removal of all the oxide ions from the central MnO_x layer of the host material, resulting in a product phase which would contain manganese cations in highly unfavorable 2-fold coordination sites. As shown in Figure 8f, the $MnO_{0.5}$ layers present in $Sr_4Mn_3O_{6.5}Cl_2$ are the most anion-deficient layers that can be constructed while maintaining a 4-fold manganese coordination, suggesting that the need to maintain a manganese coordination number of 4 limits the level of reduction that can be achieved and directs the structure of the reduced phase formed.

The polyhedral connectivity within the $MnO_{0.5}$ layers of $Sr_4Mn_3O_{6.5}Cl_2$ looks rather unusual in the context of other anion-deficient Ruddlesden−Popper phases. However, as shown in Figure 5, the resulting chains of MnO_4 tetrahedra present in the reduce oxychloride phase can be viewed as a section through the antifluorite structure[22] and can therefore be derived by close-packing arguments. In addition, while the separation between manganese centers in the edge-sharing MnO_4 tetrahedra in $Sr_4Mn_3O_{6.5}Cl_2$ appears quite short (~2.75 Å, Table 2) it is considerably larger than the separation between manganese cations in the face-sharing MnO_6 octahedra present $BaMnO_{3-x}$ phases (2.42−2.54 Å);[23] thus, there is no indication of direct Mn−Mn bonding in the reduced oxychloride phase.

Magnetism. The Curie constant observed for $Sr_4Mn_3O_{6.5}Cl_2$ over the temperature range $30 \leq T/K \leq 300$ is significantly smaller than would be expected for a 2:1 mixture of Mn^{2+} and Mn^{3+} (C_{obs} = 2.63(4) cm^3 K mol^{-1}, C_{expect} = 11.75 cm^3 K mol^{-1}). This suggests strong (antiferro)magnetic coupling exists between magnetic centers, but the lack of magnetic Bragg peaks at 5 or 300 K indicates that no long-range order exists in the temperature range studied. Given the layered nature of the crystal structure of $Sr_4Mn_3O_{6.5}Cl_2$, the observed magnetic behavior is consistent with two-dimensional magnetic order in a manner analogous to that observed in the n = 1 Ruddlesden−Popper phases $LaSrMnO_{3.5}$ and $LaBaMnO_{3.5}$.[17] These later phases undergo transitions to three-dimensional magnetically ordered states at 155 and 135 K, respectively; however, it appears that the larger interlayer separation of $Sr_4Mn_3O_{6.5}Cl_2$ (8.54 Å compared to 7.10 and 7.35 Å for $LaSrMnO_{3.5}$ and $LaBaMnO_{3.5}$, respectively)[17] weakens the interlayer magnetic coupling sufficiently to prevent three-dimensional magnetic order in the oxychloride phase.

In conclusion, it can be seen that the presence of chloride ions in the n = 3 Ruddlesden−Popper phase $Sr_4Mn_3O_{7.5}Cl_2$ directs the low-temperature reduction reaction to yield a reduced phase with highly unusual structural units — chains of edge-sharing tetrahedra. When it is combined with the structure-directing influence of halogen substitution previously seen in the $Sr_3Fe_2O_7/Sr_3Fe_2O_5Cl_2$ system,[11] this observation suggests that judicious anion substitution followed by low-temperature reduction should enable the directed synthesis of materials containing novel transition-metal oxygen networks.

AUTHOR INFORMATION

Corresponding Author

*Tel: +44 1865 272623. Fax: +44 1865 272690. E-mail: michael.hayward@chem.ox.ac.uk.

Notes

The authors declare no competing financial interest.

ACKNOWLEDGMENTS

We thank E. Suard for assistance collecting the neutron powder diffraction data.

REFERENCES

(1) Hayward, M. A.; Green, M. A.; Rosseinsky, M. J.; Sloan, J. *J. Am. Chem. Soc.* **1999**, *121*, 8843.

(2) Tsujimoto, Y.; Tassel, C.; Hayashi, N.; Watanabe, T.; Kageyama, H.; Yoshimura, K.; Takano, M.; Ceretti, M.; Ritter, C.; Paulus, W. *Nature* **2007**, *450*, 1062.

(3) Dixon, E.; Hadermann, J.; Ramos, S.; Goodwin, A. L.; Hayward, M. A. *J. Am. Chem. Soc.* **2011**, *133*, 18397.

(4) Hadermann, J.; Abakumov, A.; Adkin, J. J.; Hayward, M. A. *J. Am. Chem. Soc.* **2009**, *131*, 10598.

(5) Seddon, J.; Suard, E.; Hayward, M. A. *J. Am. Chem. Soc.* **2010**, *132*, 2802.

(6) Ruddlesden, S. N.; Popper, P. *Acta Crystallogr.* **1958**, *11*, 54.

(7) Knee, C. S.; Weller, M. T. *Chem. Commun.* **2002**, 256.

(8) Knee, C. S.; Zhukov, A. A.; Weller, M. T. *Chem. Mater.* **2002**, *14*, 4249.

(9) Knee, C. S.; Field, M. A. L.; Weller, M. T. *Solid State Sci.* **2004**, *6*, 443.

(10) Kageyama, H.; Watanabe, T.; Tsujimoto, Y.; Kitada, A.; Sumida, Y.; Kanamori, K.; Yoshimura, K.; Hayashi, N.; Muranaka, S.; Takano, M.; Ceretti, M.; Paulus, W.; Ritter, C.; Andre, G. *Angew. Chem.* **2008**, *47*, 5704.
(11) Dixon, E.; Hayward, M. A. *Inorg. Chem.* **2010**, *49*, 9649.
(12) O'Malley, M.; Lockett, M. A.; Hayward, M. A. J. *Solid State Chem.* **2007**, *180*, 2851.
(13) Larson, A. C.; Von Dreele, R. B. *Los Alamos Natl. Lab., [Rep.] LA (U. S.)* **2000**, 86−748.
(14) Leonowicz, M. E.; Poeppelmeier, K. R.; Longo, J. M. J. *Solid State Chem.* **1985**, *59*, 71.
(15) Hansteen, O. H.; Fjellvag, H.; Hauback, B. C. *J. Mater. Chem.* **1998**, *8*, 2081.
(16) Parsons, T. G.; D'Hondt, H.; Hadermann, J.; Hayward, M. A. *Chem. Mater.* **2009**, *21*, 5527.
(17) Kitchen, H. J.; Saratovsky, I.; Hayward, M. A. *Dalton Trans.* **2010**, *39*, 6098.
(18) Brese, N. E.; O'Keeffee, M. *Acta Crystallogr., Sect. B: Strucut. Sci.* **1991**, *B47*, 192.
(19) Mitchell, J. F.; Millburn, J. E.; Medarde, M.; Short, S.; Jorgensen, J. D. *J. Solid State Chem.* **1998**, *141*, 599.
(20) Seinberg, L.; Yamamoto, T.; Tassel, C.; Kobayashi, Y.; Hayashi, N.; Kitada, A.; Sumida, Y.; Watanabe, T.; Nishi, M.; Ohoyama, K.; Yoshimura, K.; Takano, M.; Paulus, W.; Kageyama, H. *Inorg. Chem.* **2011**, *50*, 3988.
(21) Retuerto, M.; Jimenez-Villacorta, F.; Martinez-Lope, M. J.; Fernandez-Diaz, M. T.; Alonso, J. A. *Inorg. Chem.* **2011**, *50*, 10929.
(22) Wells, A. F. *Structural Inorganic Chemistry*; Oxford University Press: Oxford, U.K., 1984.
(23) Adkin, J. J.; Hayward, M. A. *Chem. Mater.* **2007**, *19*, 755.